The influence of defects at the steel/concrete interface for chloride-induced pitting corrosion of naturally-deteriorated 20-years-old specimens studied through X-ray Computed Tomography

Rossi, Emanuele; Polder, Rob; Copuroglu, Oguzhan; Nijland, Timo; Šavija, Branko

DOI
10.1016/j.conbuildmat.2019.117474

Publication date
2020

Document Version
Final published version

Published in
Construction and Building Materials

Construction and Building Materials 235 (2020) 117474

Contents lists available at ScienceDirect

Construction and Building Materials

journal homepage: www.elsevier.com/locate/conbuildmat

The influence of defects at the steel/concrete interface for chloride-induced pitting corrosion of naturally-deteriorated 20-years-old specimens studied through X-ray Computed Tomography

Emanuele Rossi [a,*], Rob Polder [a,b], Oguzhan Copuroglu [a], Timo Nijland [c], Branko Šavija [a]

[a] Delft University of Technology, Faculty of Civil Engineering & Geosciences – Department of Materials & Environment, Stevinweg 1, 2628 CN Delft, The Netherlands
[b] RPCP, Fluwelensingel 106, 2806 CH Gouda, The Netherlands
[c] TNO Buildings, Infrastructures and Maritime, Stieltjesweg 1, 2628 CK Delft, The Netherlands

HIGHLIGHTS

- Eight 20-years-old corroding reinforced concrete cores are studied through X-ray CT.
- OPC-specimens had lower corrosion resistance than blended-cement specimens.
- The deepest pits are found at the outer side of the steel and close to interfacial voids.
- Interfacial voids should be considered the locations where pits propagate the most.

ARTICLE INFO

Article history:
Received 16 May 2019
Received in revised form 6 September 2019
Accepted 3 November 2019
Available online 9 November 2019

Keywords:
Reinforcement corrosion
Reinforced-concrete
X-ray computed tomography
Steel-concrete interface

ABSTRACT

Although reinforcement corrosion is a well-known issue, which are the locations of the steel/concrete interface most sensitive to pitting corrosion is still an unclear issue. In this study, X-ray computed tomography is used to characterize eight 20-years-old reinforced concrete cores naturally deteriorated due to chloride-induced corrosion. The deepest and most frequent corrosion pits were observed at the portion of the reinforcement oriented to the outdoor environment and in proximity to interfacial air voids. Therefore, the presence of interfacial air voids should be considered as a relevant factor when assessing the risk of corrosion of reinforced concrete structures.

1. Introduction

Chloride-induced corrosion of steel reinforcement is a common cause of deterioration for reinforced concrete structures [1]. It involves the dissolution of iron and the subsequent formation of iron oxides due to the presence of a chloride content at the reinforcement higher than the chloride threshold value for corrosion initiation. The chloride threshold value is defined as the critical chloride content (C_{crit}) that causes corrosion initiation and this is one of the main parameters considered when assessing the corrosion risk for reinforced concrete structures [2]. However, corrosion initiation is reported to be highly dependent on many inter-related parameters, such as the quality of the steel/concrete interface, the chemistry of the concrete pore solution, the steel potential, the orientation of the reinforcement with regard to the concrete casting direction [3]. Hence, there is indication that C_{crit} as single parameter does not adequately describe reality when assessing corrosion risk, but that it should be considered in combination with other factors, whose presence is reported to locally influence the initiation of chloride-induced corrosion [4]. Among others, these factors include macro-pores, air voids and cracks [3].

Some studies reported that defects at the steel/concrete interface (SCI) are required for initiation of corrosion of the reinforcement [5–8]. When no defects are present at the SCI, strong and dense contact between steel and concrete is reported to provide physico-chemical protection for corrosion thanks to the buffering effect given by the concrete matrix that prevents the pH to drop due to the corrosion pit formation [5]. Hence, if the number of defects at the SCI decreases, corrosion would be significantly inhibited [9]. This statement is also confirmed by Glass et al. [10], who observed that the chloride threshold value for corrosion initiation of steel increases if the percentage of air voids at the SCI decreases. However, recent studies reported that defects at the SCI did not

* Corresponding author.
E-mail address: e.rossi@tudelft.nl (E. Rossi).

https://doi.org/10.1016/j.conbuildmat.2019.117474
0950-0618/

have any influence on corrosion initiation under certain environmental conditions [11,12]. Angst et al. [4] observed by visual inspection that the location of corrosion onset did not coincide with the location of interfacial air voids. They suggest this is because the voids were not saturated. So, the lack of electrolyte at these locations could prevent corrosion to initiate. Boschmann et al. [12] found that corrosion initiation in the majority of cases did not occur at air voids in cores taken from existing structures, that were exposed in the laboratory to chloride solution. Although several studies have been conducted on the influence of interfacial defects for corrosion initiation [4–13], on-going research on the topic highlights the importance to clarify if, and how, interfacial voids may affect the chloride critical value and so initiation of corrosion.

In this study, characterization of 20-year-old reinforced concrete specimens was conducted through X-ray Computed Tomography (CT-scan or X-ray CT) and image analysis. During the last decade CT-scanning became a popular non-destructive technique for monitoring corrosion of the reinforcement in concrete. Recently, it has been used to identify and analyze location of the air voids within the concrete matrix [14], porosity of concrete [15], initiation of corrosion [16], and to characterize corrosion product at the steel/concrete interface [17]. The non-destructive principle of X-ray CT, in combination with the natural deterioration that specimens were subjected to, allowed to avoid any approximations due to destructive analysis of the SCI as well as due to corrosion acceleration under laboratory conditions (i.e. anodic polarization), which might influence how and where the corrosion occurs. The main aim of this study was to analyze and to quantify the depth and the amount of corrosion pits with regard to the presence of defects at the SCI and to the outside/inside oriented portion of the reinforcement. Also, the volume loss of steel due to corrosion after 20 years of natural exposure was quantified, and the pit distribution along the reinforcement was analyzed.

2. Materials and methods

2.1. Specimen preparation and X-ray computed tomography

In this study, eight reinforced concrete cores were analyzed through CT-scanning. The cores were drilled out of eight 20-years-old prisms cast in 1998 by Polder et al. [18] with dimensions equal to 300 mm × 100 mm × 100 mm, which were part of a larger series of around 200 specimens. The prisms analyzed in this study were cast with four different cement types (CEM I, CEM II/B-V, CEM III/B, CEM V/A), same water/binder ratio (0,55) and they were made with siliceous river material as aggregate with a maximum diameter (D_{max}) of 8 mm. Fig. 1 shows the geometrical representation of the prisms. In each prism, two groups of three smooth mild steel bars of 8 mm diameter were embedded at 10 mm and 30 mm of cover depth from the mold face. Prior to casting, each bar was prepared by light polishing with sandpaper and cleaning in acetone. A coat of cement paste and subsequently a coat of dense epoxy coating were given to both ends, leaving an exposed length of 45 mm starting at 10 mm from the top side of the prism. Each bar had an embedded length of around 80 mm. The concrete casting direction was parallel to the bars. Two activated titanium wire electrodes (Ti*) and four stainless steel bars were also part of the specimens' layout, but they were not considered in this study.

After casting, the face parallel and closer to the rebars was exposed to salt solution wet/dry cycles for 6 months, which consisted of exposing the specimens to a 3% NaCl solution for 24 h and let them dry for 6 days. After the salt/dry cycles, prisms were first stored in climate chambers for two years, and then they were exposed unsheltered to the outdoor environment of Delft, the Netherlands (temperate climate with cool summers and moderate winters), for around 17 years until sampling for this study. Electro-chemical measurements related to corrosion initiation and semi-destructive analysis (e.g. chloride profiles) were collected during the first 2.5 years [18,19] and 12 years after casting [20]. According to Polder and Peelen [19], at 26 weeks after casting the average chloride content at the reinforcement depth was higher than 2.0% by mass of cement for all the specimens (Table 1). Potential, corrosion rate and concrete resistivity related to rebars at 10 mm depth suggested that corrosion had initiated during the first year. The probability of corrosion for rebars embedded in different mixes is reported in Table 1.

Table 2 shows a summary of the properties of each prism as well as the label given to each specimen which was further analyzed in this study. Occurrence of corrosion of the selected specimens was suggested by both previous work [18–20] and visual inspections of specimens conducted at 20 years age, since in all the specimens surface rust stains and/or cracks were visible, as summarized in Table 2.

One core of 20 mm diameter was drilled out of each selected specimen. The cores were 100 mm long and they embedded one steel bar (as much centered as possible) that belonged to the group located at 10 mm of cover depth. Prior to drilling, the bottom side of the prism was marked with an arrow indicating the direction of the mold face, to keep track of which side was oriented to the outside

Table 1
Chloride content (% by mass of cement) at 10 mm depth measured at after 26 weeks of salt/dry exposure and corrosion probability of rebars at 10 mm cover depth at 52 weeks age (data from [19]). Each chloride content is the average of measurements from 6 specimens. Only specimens with w/c of 0.55 are considered.

Cement type	Chloride content at 10 mm depth in % by mass of cement (average of 6 specimens) at 26 weeks after casting	Probability of corrosion for rebars at 10 mm depth at 52 weeks after casting
CEM I	Around 3.0%	100
CEM II/B-V	Around 4.5%	100
CEM III/B	Around 2.5%	100
CEM V/A	Around 2.5%	100

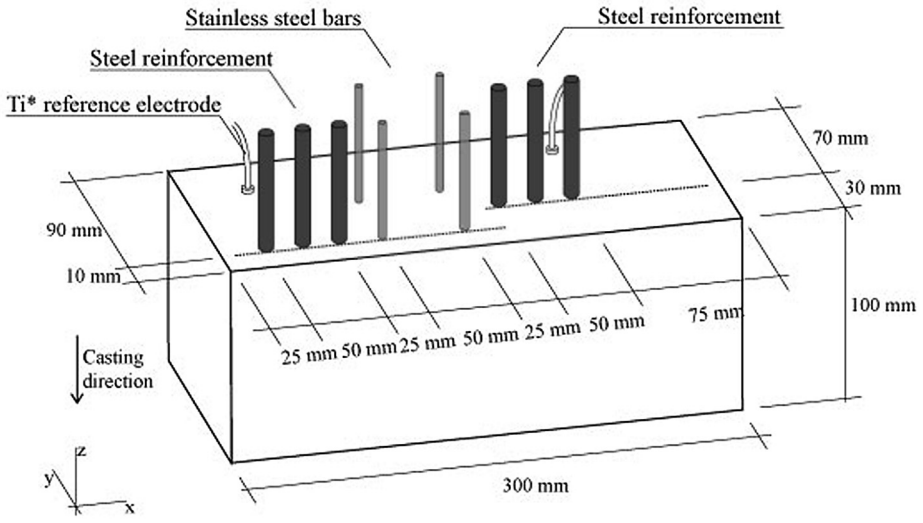

Fig. 1. Schematic representation of reinforced concrete prisms.

Table 2
Summary of properties of reinforced concrete prisms analyzed in this study: (OPC = ordinary Portland cement; FA = fly ash; BFS = blast furnace slag).

Label	Cement type	W/c	Surface state after visual inspections
1550-S1	CEM I 32.5 R OPC	0,55	Cracked and surface rust stains
1550-S2	CEM I 32.5 R OPC	0,55	Surface rust stains
1550-S3	CEM I 32.5 R OPC	0,55	Large surface rust stains
2550-S3	CEM II/B 32.5 R FA (27%) cement	0,55	Small surface rust stains
3550-S1	CEM III/B 42.5 N BFS (75%) cement	0,55	Small surface rust stains
3550-S2	CEM III/B 42.5 N BFS (75%) cement	0,55	Small surface rust stains
5550-S1	CEM V/A 42.5 N FA (25%) and BFS (25%) composite cement	0,55	Cracked and surface rust stains
5550-S2	CEM V/A 42.5 N FA (25%) and BFS (25%) composite cement	0,55	Cracked and surface rust stains

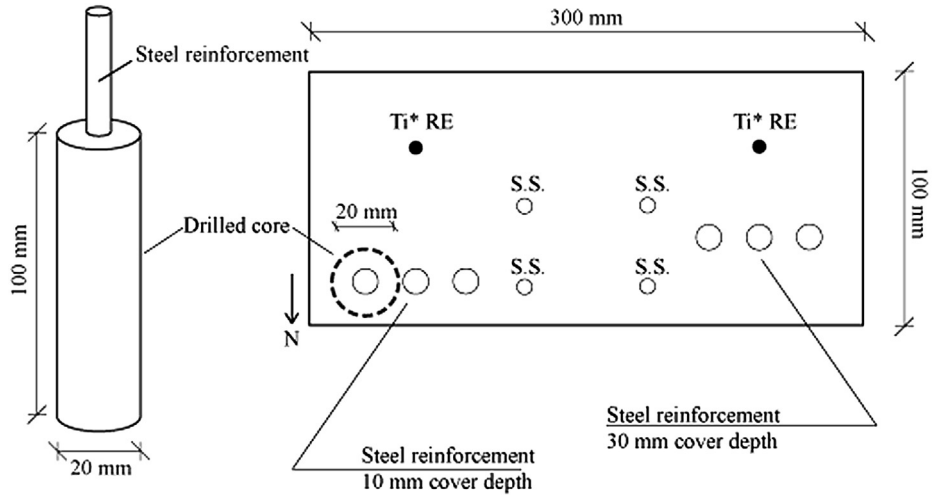

Fig. 2. schematic representation of the drilled core (left) and top view of the specimen from which the cores were drilled (right) (S.S. = stainless steel; Ti*Re = activated Titanium electrode; dotted line = drilled core; N = direction towards the outdoor environment).

(labeled as N-direction). To minimize any artificial damage potentially caused by the drilling procedure, the drilling rotation speed was kept as low as possible and it was conducted in dry conditions. The drilling procedure is represented in Fig. 2.

Fig. 3 shows the cores after drilling. 1550-S1 and 5550-S1 had visible signs of corrosion. Both cores had cracks parallel to the bar, which were filled by corrosion product. Also 5550-S2 had slightly visible cracks parallel to the steel, but no visible corrosion product at the surface. 1550-S3 and 2550-S3 did not have any crack, but some rust spots are visible at their surface. For 3550-S1, some surface rust spots are visible as well as a crack at the top side of the specimen. On the other hand, 1550-S2 and 3550-S2 did not show any sign of corrosion when observed from the outside.

After drilling, cores were kept for 72 h in a room at 20 °C and 45% RH, then CT-scans were preformed using a Phoenix Nanotom. Images were acquired at 150 kV of transmission acceleration voltage with a spatial resolution of 20 μm. The first CT-scan was taken at 10 mm from the top side of the core. Each scan was composed of 2303 slices in the height direction (Z-axis) and 2283 slices in width and depth directions (X- and Y-axis respectively). The height of the core that was scanned roughly corresponded to the exposed portion of the bar (around 45 mm). Each pixel of the performed scans contained 16 bits and displayed a grey scale value corresponding to the detected X-ray density. The reconstruction of each specimen was then performed through Datos veloCt, the software provided by the equipment manufacturer. Different components of each scan (i.e. steel, corrosion product, air

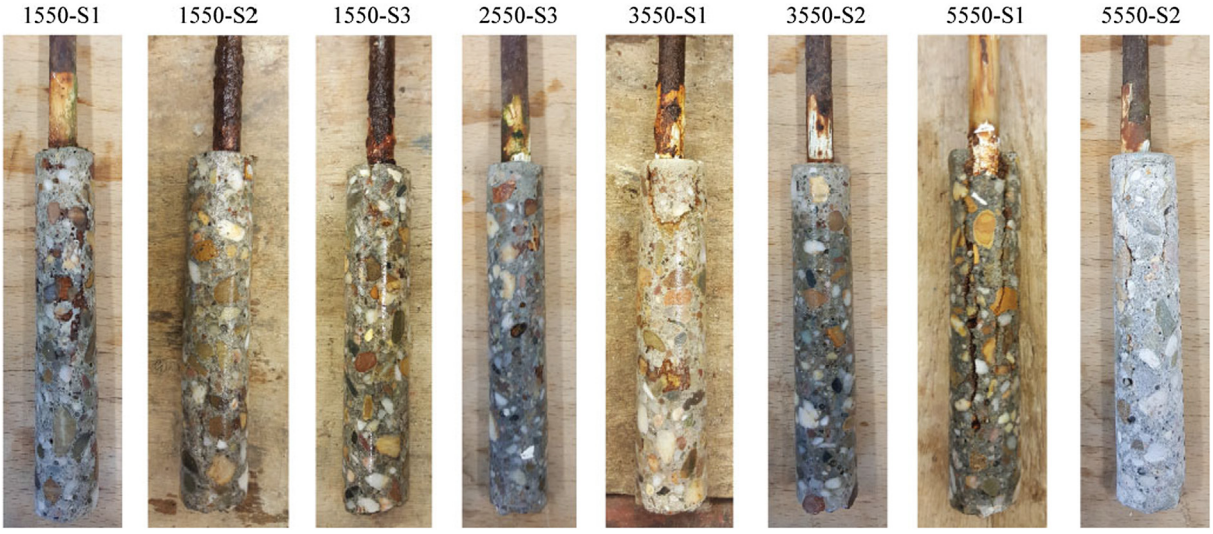

Fig. 3. Reinforced concrete cores after drilling.

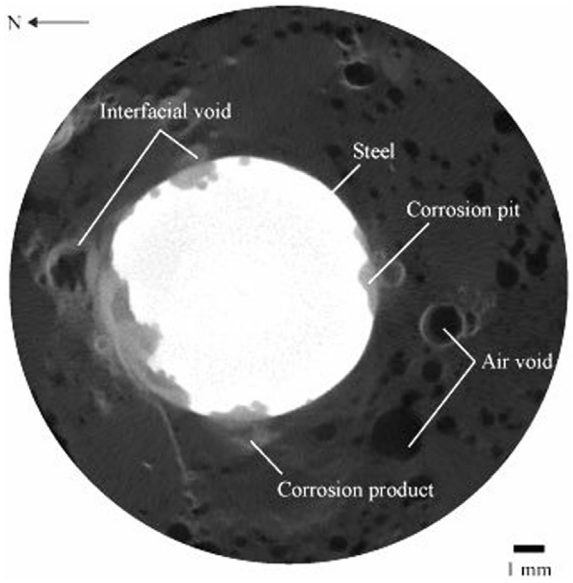

Fig. 4. CT-scan showing different phases (from 1550-S1).

voids, cracks and concrete) were segmented based on their different grey scale values using the freeware Fiji. An example of one CT-scan showing different phases of the material is shown in Fig. 4.

2.2. Steel volume loss quantification

The volume loss of steel due to corrosion was quantified for each mm of rebar length. The volume projection of each mm of rebar length was generated using the 3D Project function and then computed by the plugin 3D object counter. This latter tool allows to quantify the voxels related to the segmented component (in this case of the non-corroded steel) and to convert it into mm^3 using pixels and voxels statistics [21]. The volume for each mm section of the non-corroded steel can be quantified according to:

$$n_{vol} = n_{vox} * Z_{vox}$$

where n_{vol} is the volume of the segmented component (mm^3), n_{vox} is the number of voxels and Z_{vox} is the voxel volume (mm^3). The volume loss of steel due to corrosion, V_{loss}, was then quantified in percentage as the difference between the initial volume of the steel and the volume of non-corroded steel 20 years after casting according to:

$$V_{loss} = (V_0 - n_{vol})/V_0 * 100$$

where V_0 is the initial volume of the reinforcement (mm^3) and n_{vol} is the volume of the reinforcement 20 years after casting (mm^3). To calculate the initial volume of the reinforcement (V_0), the diameter of non-corroded portion of each specimen was measured directly from the CT-scans. The volume loss was quantified for each mm of rebar, hence resulting in a volume loss profile along the reinforcement.

2.3. Relation between defects at the SCI and corrosion pits

The relation between defects at the SCI, depth and occurrence of corrosion pits was also investigated. For each specimen, a selection of around ten 2D CT-images was analyzed. For each CT-image, pit depths were clock-wise measured at different angles from the center of the bar around 360° with 30° intervals as conducted by Sun et al. [22], as shown in Fig. 4. The depth of the pits, d, is measured by:

$$d = R_0 - R$$

where R_0 is the initial radius of the steel bar and R is the radius of the corroded steel at 20 years age. The range between 180° and 0° clock-wise, *N-direction*, indicates the direction to the mold face (i.e. the portion closer to the outside environment). After measuring pit depths, they were divided in four groups depending on their orientation (N- and S-direction) and if they were in proximity to air voids at the SCI: type 1 (T1, in orange) and type 3 (T3, in green) were indicating corrosion pits formed close to air voids at N- and S-orientation respectively. Type 2 (T2, in yellow) and type 4 (T4, in blue) were indicating pits formed where the cement paste is dense at the SCI at both the orientations (N- and S-direction respectively). An example of this distinction is shown in Fig. 5.

3. Results

3.1. Steel volume loss quantification and corrosion pit distribution

In Figs. 6–9, the volume loss of steel along the length of the reinforcement for each specimen is reported.

Fig. 6 (left, 1550-S1) shows high volume loss of 2–11% due to corrosion along the whole length of the bar, except for a few slices at the bottom of the bar. On the other hand, Fig. 6 (right, 1550-S2) shows a low level of corrosion along the whole length of the rebar (around 1%), with exceptions for only a few slices where the maximum volume loss reaches around 5% (at the top of the bar) and around 3% (at 15 mm length). 1550-S3 and 2550-S3 (Fig. 7) have different volume losses equal to around 3.5% and 2% respectively. Both specimens are subjected to relatively deep pits that cause a maximum localized volume loss of around 9% for both. Qualitatively, pits from 1550-S3 seem wider and more superficial, while pits present in 2550-S3 look deeper and more localized. 3550-S1 and 3550-S2 (Fig. 8) have a similar corrosion pattern along the rebar length. For both, the total volume loss is relatively low, equal to around 1%. No significant corrosion for most of the length of the bars is visible, with most of the slices that register volume losses lower than 1%, except for a few localized pits, leading to a highest local volume loss of around 4%. The sides of 3550-S1 seemed

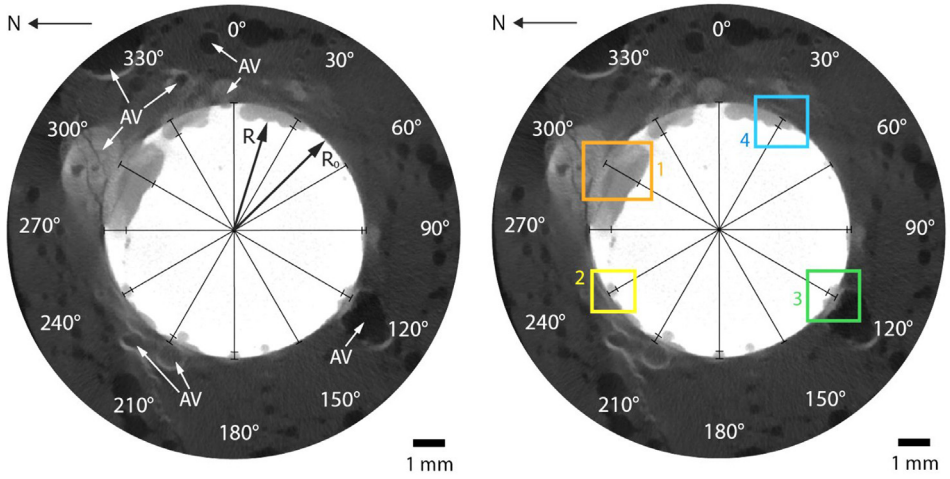

Fig. 5. (left) Depth and orientation of corrosion pits (AV = air voids). (right) corrosion pit distinction: N-oriented pit in proximity of an air void (type-1, orange); N-oriented pit coincident to dense cement paste at the SCI (type-2, yellow); S-oriented pit in proximity of an air void (type-3, green); S-oriented pit coincident to dense cement paste at the SCI (type-4, blue). (For interpretation of the references to colour in this figure legend, the reader is referred to the web version of this article.)

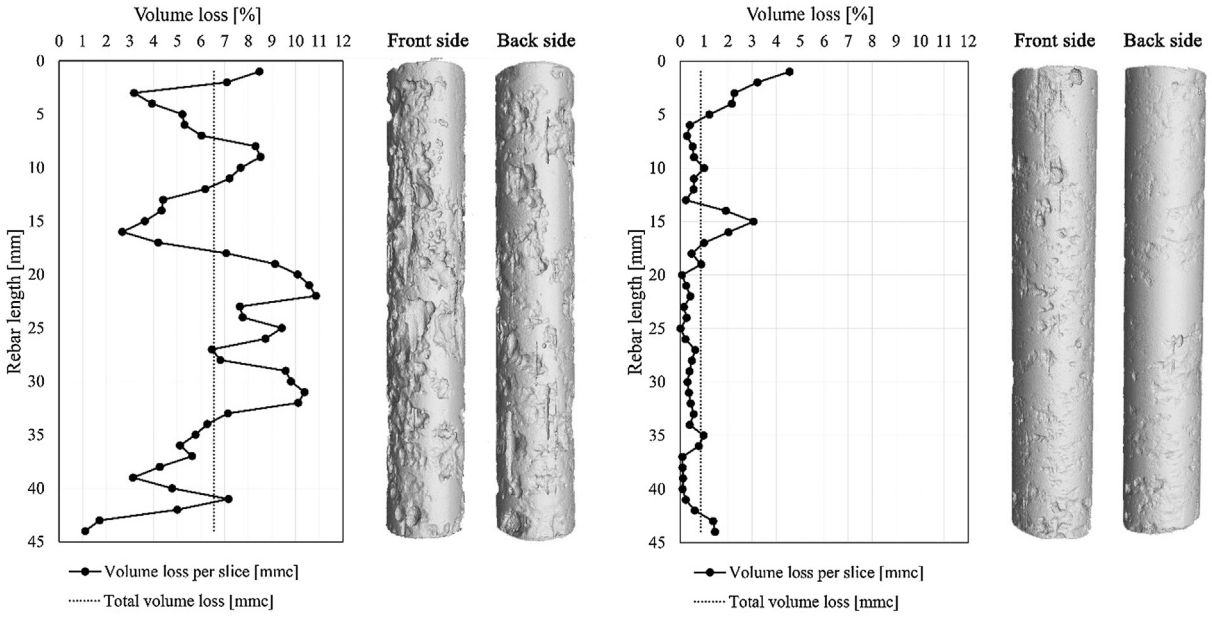

Fig. 6. 1550-S1 (left) and 1550-S2 (right) steel reinforcement render and volume loss per 1-mm slice along the bar length. Front side = N-oriented.

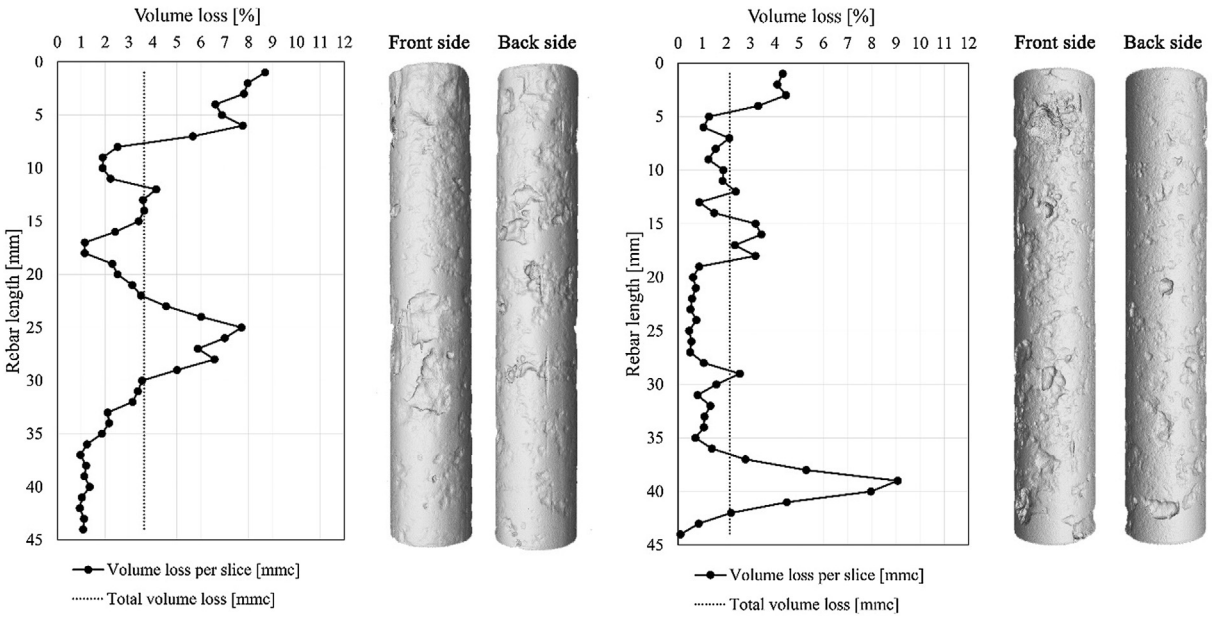

Fig. 7. 1550-S3 (left) and 2550-S3 (right) steel reinforcement render and volume loss per 1-mm slice along the bar length. Front side = N-oriented.

degraded by more superficial pits than those of 3550-S2, for which pits look deeper but less frequent. 5550-S1 and 5550-S2 (Fig. 9) had different progress of corrosion along their length, in terms of both the distribution of corrosion pits and the total volume loss. The former specimen lost around 4.5% of steel in total, while the latter one lost around 3%. 5550-S1 was heavily cracked, and it shows a relatively uniform volume loss along the whole length of the reinforcement, with lowest and highest points of around 3% and 7% respectively. On the other hand, 5550-S2 was not heavily cracked, and the progress of volume loss the bar is more like the other specimens, with lower volume losses for most of the length (of around 2%) alternated by localized deep pits, leading to a maximum volume loss of around 7%. The average volume loss along the reinforcement for each specimen is reported in Table 3. It appears that specimens cast with blended cements had lower volume loss due to corrosion than specimens cast with Ordinary Portland cement. 3550-S1 and 3550-S2 had a volume loss equal to 1.10% and 1.33% respectively, around six times lower than the volume loss of 1550-S1 (equal to 6.55%), which was found to be the most corroded. Also 2550-S3 had a relatively low volume loss equal to 2.14%, comparable to CEM III/B specimens. On the other hand, CEM V/A specimens had the highest volume loss considering blended cement specimens only, with 4.60% and 3.12% for 5550-S1 and 5550-S2 respectively.

3.2. Relation between defects at the SCI and corrosion pits

The relation between corrosion pit depths, pit orientation and the presence of defects at the SCI is shown in the boxplot reported in Fig. 10. Comparing T1 to T2 and T3 to T4, the influence of air

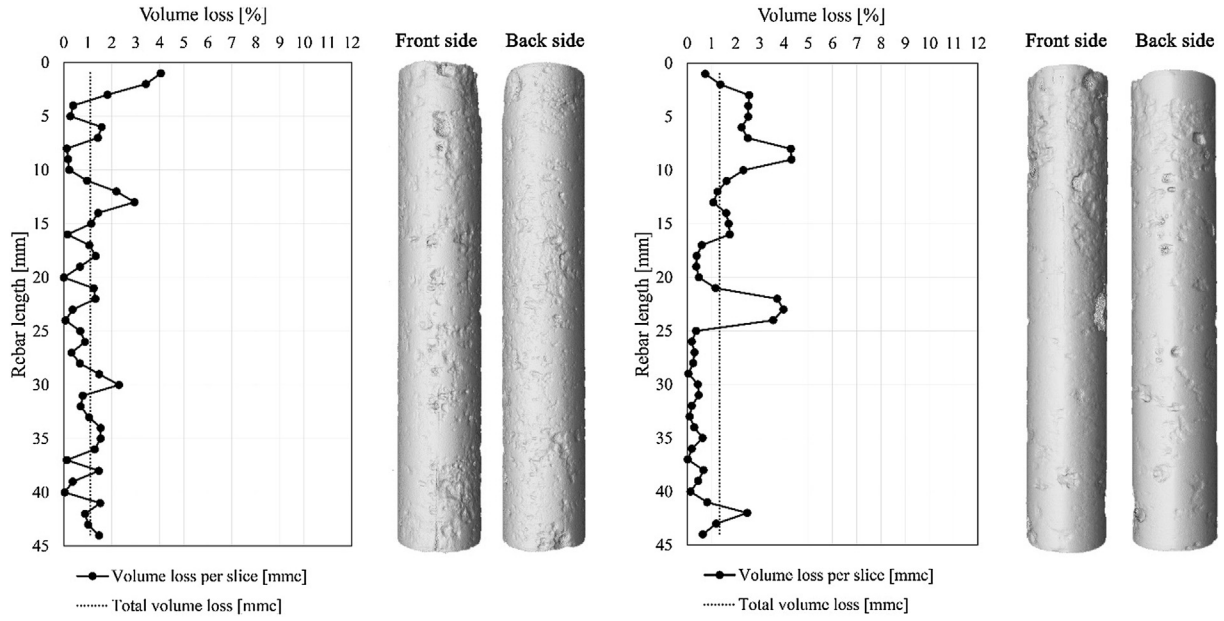

Fig. 8. 3550-S1 (left) and 3550-S2 (right) steel reinforcement render and volume loss per 1-mm slice along the bar length. Front side = N-oriented.

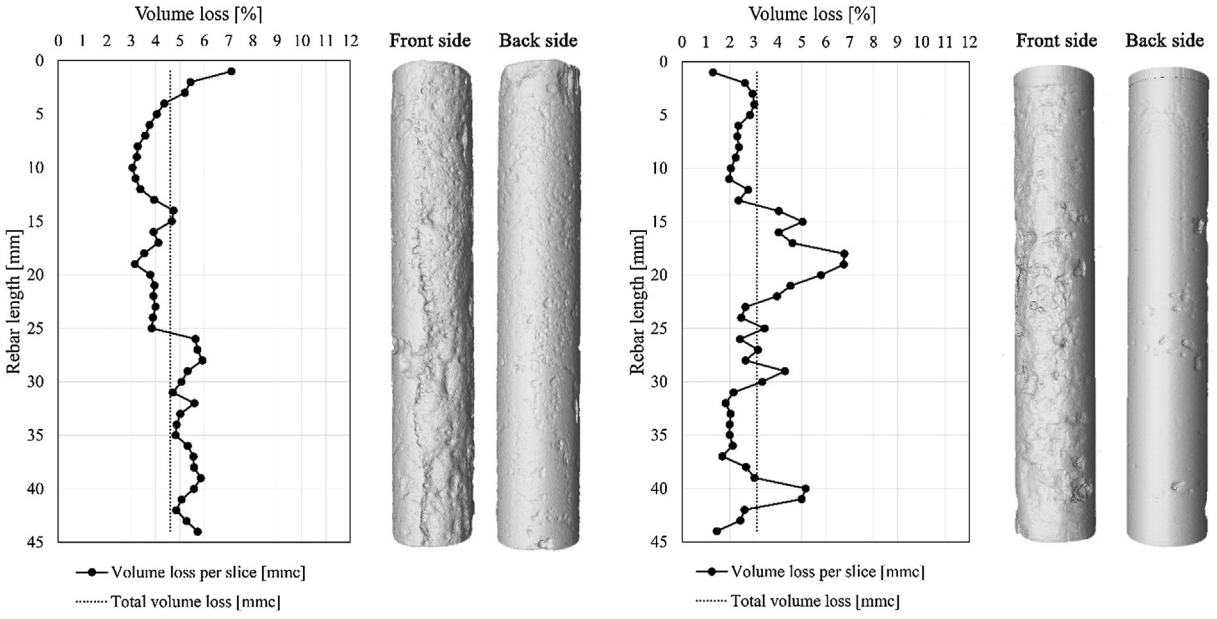

Fig. 9. 5550-S1 (left) and 5550-S2 (right) steel reinforcement render and volume loss per 1-mm slice along the bar length. Front side = N-oriented.

Table 3
Average volume loss of steel reinforcement (%) calculated through image analysis.

Specimen	Volume loss (%)
1550-S1	6.55
1550-S2	0.86
1550-S3	3.64
2550-S3	2.14
3550-S1	1.10
3550-S2	1.33
5550-S1	4.60
5550-S2	3.12

voids at the SCI on corrosion pit depth can be analyzed. Pits at voids (T1 and T3) were generally found to be deeper than corresponding pits with similar orientation but which are formed where the cement paste at the SCI is dense (T2 and T4). This statement is valid for all specimens except for 3550-S1 and 5550-S1. However, in the former case only a few air voids were present at the SCI, hence compromising the comparison with other specimens. 5550-S1 was heavily cracked on the N-oriented side. In this latter case, the cracking probably led to higher and more frequent ingress of water along the bar, transforming the mechanism of pitting corrosion into a more general corrosion oriented to the cracked side, as suggested by Fig. 9.

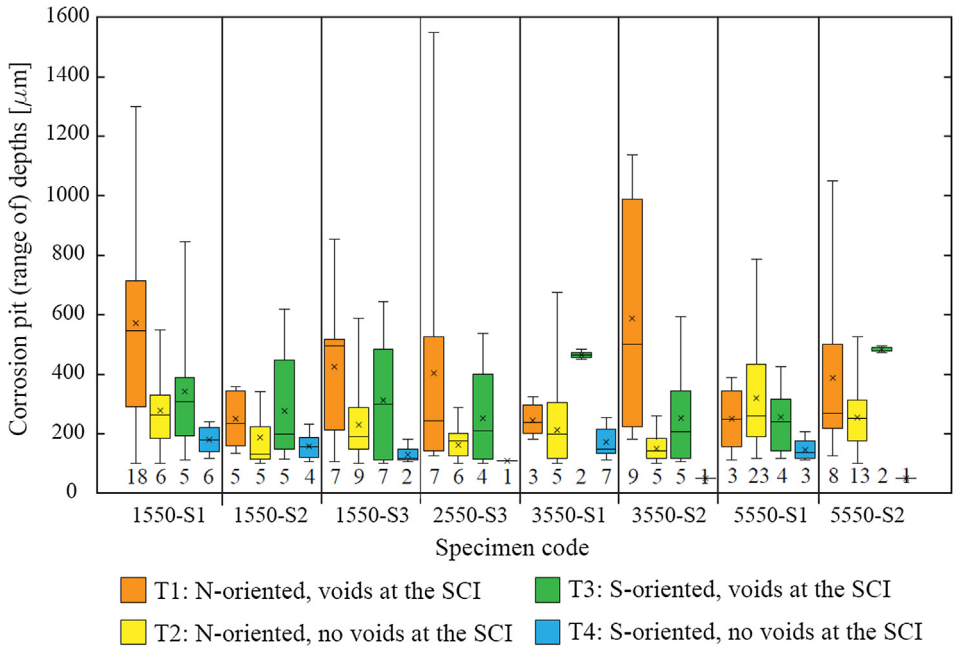

Fig. 10. Range of depth of types of corrosion pits (μm) with outside/inside orientation and proximity to concrete defects at the SCI. The top, middle and bottom line of the boxes correspond to the 75-, 50- and 25-percentile value (x_{75}, x_{50} and x_{25}) respectively. The whiskers show the minimum and maximum values. The number below each series represents the number of pits of each specimen.

At the same time, the influence of the steel orientation can be investigated comparing T1 to T3 and T2 to T4. For most of the specimens, N-oriented pits are deeper than S-oriented pits, likely due to more frequent exposure to wet and dry cycles during outdoor exposure due to the closer proximity of this side to the environment. Also, higher ingress of harmful agents (i.e. carbon dioxide) may have made the N-oriented side of the reinforcement more sensitive to corrosion. Generally, the combination of closer exposure to the outside and presence of air voids (i.e. T1 pits) revealed to be the most aggressive conditions for corrosion pits to firstly form and then to grow; on the contrary, the S-oriented side of the reinforcement revealed to be the least corroded side, particularly when no air voids at the SCI were found (T4). Based on the findings of this study, the main influencing factor for corrosion pits to form and to grow is the presence of air voids at the SCI, while less deep pits (or none) are found when the cement paste is dense around the steel bar. The relation between corrosion pits and interfacial voids is also visible in Figs. 11 and 12, where one vertical CT-scan for each specimen is reported. Especially for 1550-S1, 2550-S2, 3550-S2 and 5550-S2, relatively deep pits (around 1 mm) coincide with interfacial voids, while pits are less deep and less frequent when the steel is surrounded by cement paste.

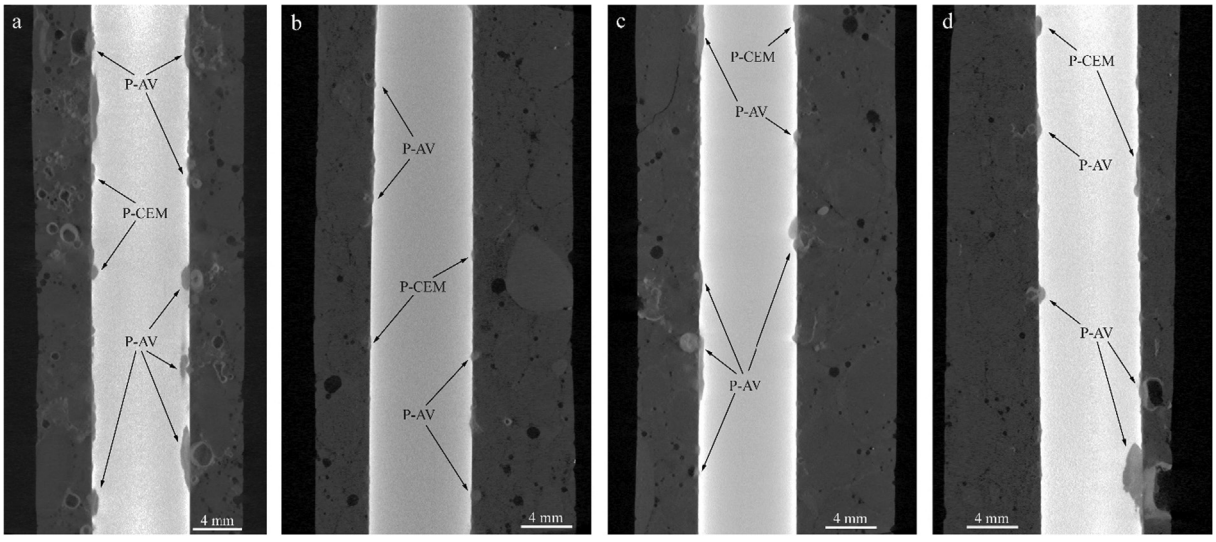

Fig. 11. Vertical CT-scans of 1550-S1 (a), 1550-S2 (b), 1550-S3 (c), 2550-S2 (d) (P-AV = Pit coincident to interfacial Air Void; P-CEM = Pit at compact Cement paste at the steel-concrete interface).

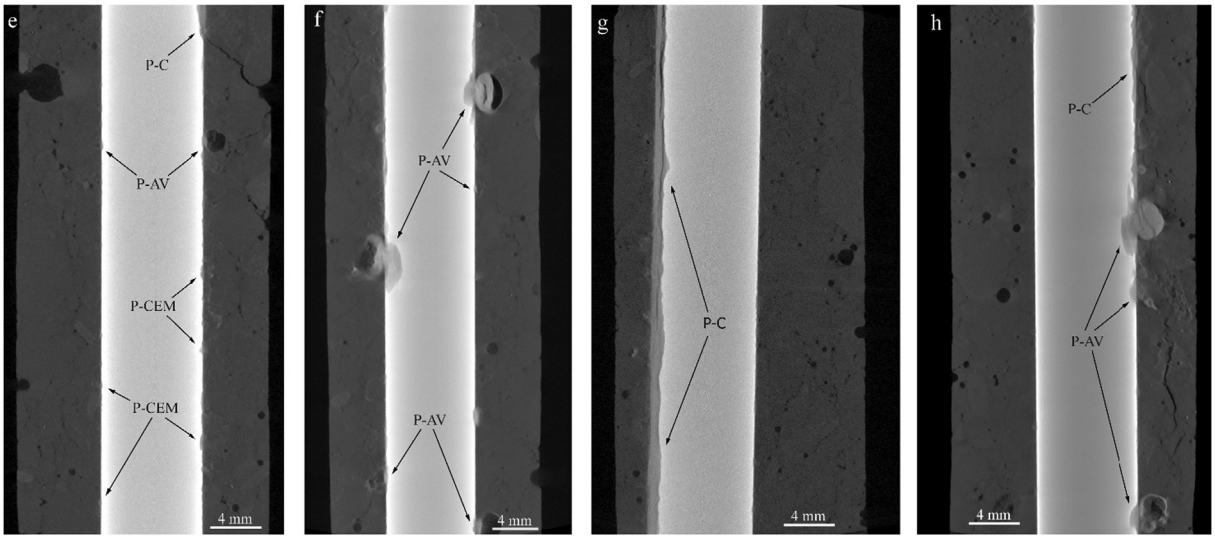

Fig. 12. Vertical CT-scans of 3550-S1 (e), 3550-S2 (f), 5550-S1 (g), 5550-S2 (h) (P-AV = Pit coincident to interfacial Air Void; P-C = Pit coincident to Crack; P-CEM = Pit at compact Cement paste at the steel-concrete interface).

4. Discussion

4.1. On the influence of concrete properties on corrosion behavior

Generally, blended cements make the concrete microstructure denser than OPC, improving chloride penetration resistance and concrete resistivity and, consequently, the corrosion resistance of the mix [19]. Similar improvements can be achieved by lowering the water/binder ratio of the concrete [4]. In this study, quantitative image analysis of CT-scans has shown that specimens cast with OPC generally had higher volume loss due to corrosion than specimens cast with blended cements. 3550-S1 and 3550-S2 were the least corroded, with around 1% of average volume loss and localized volume loss never higher than 4%. On the other hand, 1550-S1 and 1550-S3 had 6.5% and 3.5% of average volume loss respectively, with localized volume losses up to 11% and 9% respectively. Similar differences between volume loss of bars in concrete cast with CEM I and CEM III/B are in line with what was observed by Pacheco [20], who quantified the volume loss of reinforcement through visual inspections and volume estimation. A lower average volume loss of 2.5% was found also for 2550-S3, apart from the bottom part of the bar where a localized volume loss up to 9% was observed. Recently, Stefanoni et al. [23] observed that the more porous the medium around the steel reinforcement, the more aggressive corrosion occurs due to the dual role of the pore structure (in terms of transport limitations and inhomogeneity of the interfacial zone). Since blended cements lead to a denser microstructure than that of OPC, it is not surprising that, on average, rebars embedded in OPC-based cores had the highest volume loss. The highest average volume loss for blended cement specimens was measured for 5550-S1, equal to 4.6%. However, this specimen was heavily cracked, and corrosion probably accelerated after cracking, that caused differences of average volume loss with 5550-S2, which lost 3% of steel volume. Similar observations were reported by Sun et al. [22], who studied the amount of corrosion with regard to exposure side and presence of cracks of anodically-polarized reinforced concrete cores through X-ray CT. In their study, Sun et al. [22] observed that significant corrosion product formed at the steel surface where penetrating cracks occurred, whereas in non-cracked portions of the specimens the corrosion product accumulation was insignificant. Similarly, Dong et al. [24] observed through X-ray CT analysis of corroding rebars that corrosion tends to occur at the damaged (i.e. cracked) locations of the SCI. Furthermore, the uniform volume loss distributed along the rebar length of 5550-S1 is in line with the findings of Zhang et al. [25], who demonstrated a transition from pitting to generalized corrosion in reinforced concrete with cracks wider than 1.5 mm. Even though 1550-S2 was cast with OPC, it had the lowest average volume loss of all the specimens, equal to 0.86%. Since this volume loss is significantly lower than that of the other cores and especially than that of cores with same composition (1550-S1 and 1550-S3), doubts were raised about the water/binder ratio of this prism. Indeed, during the 20 years after casting, specimens were re-located several times and some may have been mislabeled. Specimens were then re-identified non-destructively, as described more in detail elsewhere [20]. It might be the case that, for 1550-S2, the identification of its water/binder ratio was not accurate. In this way, 1550-S2 would have been cast with lower water/binder ratio. Since lower water/binder ratio improves the corrosion resistance of concrete [3], it would explain why 1550-S2 had, unexpectedly, the lowest volume loss of reinforcement. Another possible explanation for this finding could be that 1550-S2 had less frequent interfacial defects than 1550-S1 and 1550-S3, as qualitatively suggested by Fig. 11b. Since in this study defects and voids at the SCI were the most sensitive locations for corrosion propagation, less frequent interfacial defects might improve the corrosion resistance and, therefore, lower the steel volume loss due to corrosion. It must be specified that volume losses of steel quantified through image analysis could be different from reality due to segmentation inaccuracies and resolution limitation, as reported by others [16]. Nevertheless, since specimens were subjected to equal image acquisition and processing, potential drawbacks related to compare one test to another are considered negligible.

4.2. On the influence of interfacial defects on chloride-induced localized corrosion behavior

Defects at the SCI are often reported to be required for initiation of corrosion since good adhesion at the steel/concrete interface limits both chlorides and oxygen to reach the reinforcement. Furthermore, a dense cement paste around the steel provides buffering against pH drop caused by corrosion pit formation, which increases the corrosion resistance of these locations of the SCI

[27]. Angst et al. [4] studied corrosion initiation of bars embedded perpendicularly to the concrete casting direction. They observed that corrosion did not start at the locations of the steel/concrete interface where the highest chloride content occurred. On the contrary, the back side (i.e. the side farther from the outside environment) of the reinforcement was the most corroded, due to imperfections and formation of gaps caused by plastic settlement and collection of bleeding water, which are influencing factor for corrosion initiation also reported by others [5,26]. Higher local water/binder ratio and porosity might also weaken the interface of the bottom side of the reinforcement, making it more sensitive to corrosion initiation [27,28]. However, Angst et al. [4] observed that corrosion never initiated at the locations where air voids were present at the SCI, which they explained by those voids were never saturated. On the contrary, Glass et al. [10] reported that reducing the percentage of interfacial voids, the critical chloride content for corrosion initiation increased, hence the corrosion resistance. According to them, the dissolution of buffering solids of the cement paste (CH and C-S-H) releases hydroxyl ions that prevent a local reduction of the pH at the SCI (due to corrosion pit formation), inhibiting corrosion initiation and increasing the corrosion resistance of those locations [5,29,30]. Thus, in presence of electrolyte and a certain chloride content, defects at the SCI would be the most sensitive locations because they cannot provide this buffering effect [9].

In this work, X-ray Computed Tomography of concrete cores with naturally corroded rebars showed that macro-defects at the SCI (i.e. air voids) appear to be the most relevant factor governing the corrosion propagation of the reinforcement, since for every air void that was found at the SCI, at least one corrosion pit was also found in its proximity. Furthermore, compared to corrosion pits formed where the cement paste is compact around the reinforcement, those formed close to air voids are generally deeper. The results of this study are also in line with what was pointed out by Glass et al. [10] about the inversely proportional relation between corrosion resistance and percentage of interfacial voids. Indeed, only a few interfacial voids were observed for the least corroded specimens (i.e. 3550-S1). As pointed out by Christodoulou [9], these voids need to be (or to have been) partially or completely saturated. Fig. 13 shows a BSE (back-scatter electron) image obtained with a Philips XL30 ESEM, acquired at 20 kV acceleration voltage, where an interfacial void partially filled by corrosion product is visible. Interestingly, it seems that the void gets gradually and concentrically filled from the edges to the center, suggesting on-going precipitation of iron oxides. Corrosion product might also be transported to the edges of the interfacial void through, most likely, a liquid that penetrated the defect. If subjected to wet and dry conditions, ingress and drying of solution might cause the corrosion product to mix with the liquid and migrating to the edges of the void. Although it is out of the scope of this study to analyze how corrosion product propagates into air voids at the SCI, Fig. 13 might suggest that, under certain conditions, interfacial voids get partially or completely filled by a liquid. Consequently, they become sensitive locations for corrosion initiation, as image analysis of CT-scans suggested.

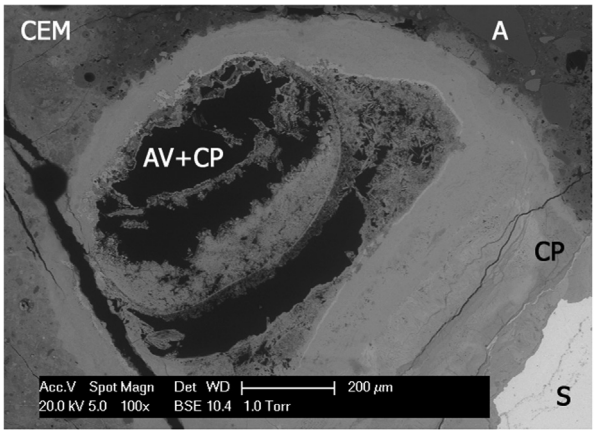

Fig. 13. BSE image of corrosion product penetrating an interfacial air void from 5550-S2 (S = steel; CP = corrosion product; A = aggregate; CEM = cement paste; AV = air void).

Corrosion initiation at interfacial voids were also visible in the study of Van Steen et al. [16], who performed X-ray CT at certain time intervals in combination with acoustic emission to localize the corrosion initiation sites in reinforced concrete specimens subjected to anodic polarization. CT-scans of their study clearly show that corrosion firstly initiates where entrapped voids at the steel/-concrete interface are present. Once initiated, corrosion pits tend to get deeper at those locations, as Fig. 10 suggested. This fact might be related to the higher availability of oxygen and electrolyte coincident to the presence of the defects. Also, dense cement paste around the reinforcement might provide a physic-chemical barrier that blocks the dissolution of iron [26]. Interfacial voids would be locations where corrosion product can be accommodated, with no constraint from the surrounding cement paste and, so, allowing corrosion pits to get deeper. A similar mechanism was observed by Šavija et al. [17], who studied corrosion progress of anodically-corroded reinforced concrete cores through X-ray CT. In their study, Šavija et al. [17] observed that presence of interfacial open spaces (i.e. macro air voids) caused non-uniformities of the corrosion layer to occur. Localized volume loss in proximity to interfacial voids was also observed by Ebell et al. [31], who coupled electrochemical measurements and X-ray CT analysis on corroding reinforced concrete specimens. In their study, corrosion product penetrating into an air void with consequent formation of a corrosion pit is shown, even though the air void is not directly adjacent to the steel reinforcement. It looks that pits are formed at the locations where corrosion product can penetrate the most, hence where the least constrain from the surrounding matrix is provided. This finding is in line with what has been recently proposed by Stefanoni et al. [23], who observed that the higher the porosity of the medium around the steel reinforcement, the higher the amount of corrosion.

Corrosion initiation of the steel rebars analyzed in this study occurred within the first two years after casting [18–20]. Corrosion propagated many years before the specimens were tested, as suggested by the state of the rebars shown by the CT-scans (Figs. 6–9). The main finding of this study was that the deepest corrosion pits occurred in proximity to interfacial air voids (Figs. 10–12). This fact might be related to the influence that interfacial voids have on either corrosion initiation or on corrosion propagation. On the one hand, it might be possible that the deepest pits are those that initiated the earliest. In this case, interfacial voids would be the most sensitive locations for corrosion initiation based on the findings of this study. However, this scenario is based on the assumption that the corrosion rate would be uniform along the whole bar during the whole service-life. This might not be entirely correct since it is likely that the corrosion rate of the pits might be influenced, for instance, by the local chloride content, the oxygen supply and the availability of electrolyte. Also, pit growth might be mitigated and even interrupted if no oxygen or electrolyte would be continuously supplied, resulting in pit re-passivation. Therefore, concluding that interfacial voids are the most sensitive locations for corrosion initiation might be premature. On the other hand, interfacial air voids might create the preferential scenario for corrosion propagation without any influence on the corrosion initiation phase. In other words, superficial pits might initiate along

the whole length of the reinforcement where the chloride content is higher than the critical threshold value, regardless the presence of interfacial voids. Pits at interfacial voids might then get deeper due to, for instance, no buffering effect provided by the dense cement paste around the steel, less constraining accommodating space for corrosion product to expand, and higher availability of oxygen and electrolyte at those locations (under partially or completely saturated conditions). Since interfacial voids would create the preferential conditions for pits to get deeper, the growth of adjacent pits might be also mitigated if not even re-passivated due to, for instance, the cathodic current flow present at the surroundings of the pit growing at interfacial voids. This might be also qualitatively suggested by Figs. 12 and 13, which show that deep pits are relatively distant from each other (around 5 to 15 mm, especially for 1550-S3, 2550-S3, 3550-S2 and 5550-S2). This mechanism suggests that the most aggressive corrosion propagation would take place in proximity to interfacial voids, resulting in consequent highest steel volume loss. The presence of interfacial voids should be then considered as a detrimental factor for the corrosion propagation resistance in reinforced concrete. Nevertheless, since the state of the rebars in this study did not allow to observe corrosion initiation during time, the influence of interfacial voids on corrosion initiation remains an open question, for which more research is highly recommended.

In this study, it was also observed that the side of the reinforcement closer to the outside environment was more corroded than the side exposed to the inside concrete, contrary to what was reported by other authors [4,32]. Angst et al. [4] observed that in bars oriented perpendicularly to the concrete casting direction, the side of the reinforcement more sensitive to corrosion was the bottom side. In this study, the reinforcement was oriented in parallel to the concrete casting direction. In so doing, concrete casting did not likely cause localization of defects at the inside-oriented side of the bars, e.g. due to plastic settlement and water bleeding. Since the quality of the SCI could be ideally considered the same for the two sides of the bars of this study, it is not surprising that the side exposed to the outside conditions would have been subjected to more aggressive corrosion due to, for instance, higher availability of the electrolyte, more frequent wet/dry cycles and higher ingress of harmful agents (i.e. chlorides). It must be specified that the steel bars had 10 mm cover depth, which is not representative for good practice. It is likely that for higher cover depths (e.g. 30–50 mm), the differences between the two sides in terms of exposure conditions could be negligible since the concrete cover would provide a much thicker barrier against electrolyte ingress and wet/dry cycles. Considering reinforcement oriented perpendicularly to the casting direction, the bottom side of the steel would likely be the most sensitive portion for corrosion to initiate because of a higher number of defects created by casting and settlement, as stated by Angst et al. [4]. Also, specimens studied in this work were 20 years old and corrosion had already propagated considerably. However, it was assumed that the locations where pits were observed through CT-scans were the locations where pits also initiated. Studying through X-ray CT specimens in which corrosion just initiated would probably give even more insights about how corrosion initiation is influenced by interfacial voids and, thus, it is highly recommended.

In summary, 20 years after casting and intense but short term exposure to chloride and subsequent outdoor environment, steel bars embedded in blended cement concretes had generally lower volume loss due to corrosion than those embedded in OPC concrete. In the case of significantly cracked concrete, a transition from pitting to general and crack-oriented corrosion was suggested based on CT-scans of one of the specimens (i.e. 5550-S1). Furthermore, this study shows that interfacial voids coincided to the locations where corrosion had become the deepest. Through image analysis, it was observed that at every location where an air void was present at the SCI, a corrosion pit was also present close by. If a certain chloride content is present at the SCI and concrete is (partially or completed) saturated, interfacial voids should be considered detrimental corrosion sites.

5. Conclusions

From this study, the following major conclusions can be drawn:

1. OPC specimens had developed corrosion generally stronger than blended cement specimens in terms of volume loss of the reinforcement after 20 years. More precisely, the bars had increasing volume loss according to the following order of cement type which they were cast with: CEM III/B, CEM II/B-V, CEM V/A, CEM I.
2. The deepest corrosion pits were found in proximity to interfacial air voids. Furthermore, at every location where a void was observed at the SCI, a corrosion pit was also visible close by. Interfacial air voids were the locations where the most aggressive corrosion propagation occurred, with consequent highest volume loss of the steel reinforcement.
3. The side of the reinforcement closer to the outside generally had deeper corrosion pits than the side exposed to the inner concrete. However, in this study bars were cast parallel to the concrete casting direction and at 10 mm of cover depth. For bars cast perpendicularly to the concrete casting direction, a more porous bleed water zone would be formed at the underside of the rebar, as reported by others [32]. Since interfacial defects seemed to be the most dominant locations influencing the corrosion resistance of the reinforcement bars, it is likely that the underside of the steel would be the most sensitive to corrosion attack. For thicker cover depth, as it is common use in practice, the influence of the proximity to outdoor conditions and consequently the exposure to wet/dry cycles would likely not be as marked as it was in this study, which should be anyway considered as relevant factor for lab-scale experiments with limited cover depth.
4. In cracked concrete, the most corroded side of the reinforcement was found along the whole length of the bar and oriented at the side towards the crack (i.e. 5550-S1). This finding confirms a transition from pitting to more general corrosion as already observed by previous studies [25]. Since for 5550-S1 occurrence of pits in proximity to interfacial defects was less pronounced than that of non-cracked specimens, it is likely that occurring cracks are the leading factor about influencing how and where corrosion would propagate the most.

Declaration of Competing Interest

The authors declare that they have no known competing financial interests or personal relationships that could have appeared to influence the work reported in this paper.

Acknowledgements

The authors would also like to thank Mr. Arjan Thijssen for his assistance with the Environmental Scanning Electron Microscope analysis and X-ray computed tomography experiments.

References

[1] L. Bertolini, B. Elsener, P. Pedeferri, R.B. Polder, Corrosion of Steel in Concrete: Prevention, Diagnosis, Repair, Wiley-VCH Verlag GMBH & Co., Weinheim, 2004.

[2] U. Angst, B. Elsener, C.K. Larsen, Ø. Vennesland, Critical chloride content in reinforced concrete – a review, Cem. Concr. Res. 39 (2009) 1122–1138.
[3] U. Angst, M. Geiker, A. Michel, et al., The steel-concrete interface, Mater. Struct. 50 (2017) 143.
[4] U. Angst et al., Chloride induced reinforcement corrosion: electrochemical monitoring of initiation stage and chloride threshold values, Corros. Sci. 53 (2011) 1451–1464.
[5] T. Soylev, R. Francois, Corrosion of reinforcement in relation to presence of defects at the interface between steel and concrete, J. Mater. Civ. Eng. 17 (2005) 447–455.
[6] T. Yonezawa, V. Ashworth, R. Procter, Pore solution composition and chloride effects on corrosion of steel in concrete, Corros. Eng. 44 (7) (1988) 489–499.
[7] T. Mohammed, N. Otsuki, M. Hisada, Corrosion of steel bars with respect to orientation in concrete, ACI Mater. J. 96 (2) (1999) 154–159.
[8] T. Mohammed, N. Otsuki, H. Hamada, T. Yamaji, Chloride-induced corrosion of steel bars in concrete with presence of gap at the steel-concrete interface, ACI Mater. J. 99 (2) (2002) 149–156.
[9] C. Christodoulou, G. Glass, Towards rendering steel reinforced concrete immune to corrosion, Australasian Corrosion Association 2012 Annual Meeting, Melbourne, Australia, 11-14 November, 2012. paper 159, 11pp.
[10] G. Glass, B. Reddy, L. Clark, Making reinforced concrete immune from chloride corrosion, Constr. Mat. 160 (2007) 155–164.
[11] U. Angst, Chloride induced reinforcement corrosion in concrete; concept of critical chloride content—methods and mechanisms PhD thesis, Norwegian University of Science and Technology, NTNU, Trondheim, 2011.
[12] C. Boschmann Käthler, U.M. Angst, B. Elsener, Towards understanding corrosion initiation in concrete – influence of local concrete properties in the steel-concrete interfacial zone, Proc. 5th Int. Conf. Concrete Repair, Rehabilitation and Retrofitting – ICCRRR, 2018, Cape Town, South Africa; MATEC web of conferences, 2018.
[13] T. Mohammed, N. Otsuki, H. Hamada, Corrosion of steel bars in cracked concrete under marine environment, J. Mater. Civil. Eng. 15 (5) (2003) 460–469.
[14] H.E. Martz, D.J. Schneberk, G.P. Roberson, P. Monteiro, Computerized tomography analysis of reinforced concrete, ACI Mat. J. 90 (3) (1993) 259–264.
[15] K. Wan, Q. Xu, L. Li, W. Sun, 3D porosity distribution of partly calcium leached cement paste, Constr. Build. Mater. 48 (2013) 11–15.
[16] C. Van Steen, L. Pahlavan, M. Wevers, E. Verstrynge, Localisation and characterisation of corrosion damage in reinforced concrete by means of acoustic emission and X-ray computed tomography, Constr. Build. Mater. 197 (2019) 21–29.
[17] B. Savija, M. Lukovic, S.A.S. Hosseini, J. Pacheco, E. Schlangen, Corrosion induced cover cracking studied by X-ray computed tomography, nanoindentation, and energy dispersive X-ray spectrometry (EDS), Mater. Struct. 48 (7) (2015) 2043–2062.
[18] R.B. Polder, P. Russo, Concrete resistivity, corrosion potential and corrosion rate at young age as a function of cement type, 98-BT-R1664 (1998), TNO Building and Construction Research, Rijswijk, TNO.
[19] R.B. Polder, W.H.A. Peelen, Characterisation of chloride transport and reinforcement corrosion in concrete under cyclic wetting and drying by electrical resistivity, Cem. Concr. Compos. 24 (2002) 427–435.
[20] J. Pacheco, Corrosion of steel reinforcement in 12 years old concrete: inspection, evaluation and electrochemical repair of corrosion Master of Science thesis, Delft University of Technology, Materials & Environment, Delft, 2010.
[21] B. Dong, W. Ding, S. Qin, G. Fang, Y. Liu, P. Dong, S. Han, F. Xing, S. Hong, 3D visualized tracing of rebar corrosion-inhibiting features in concrete with a novel chemical self-healing system, Constr. Build. Mater. 168 (2018) 11–20.
[22] H. Sun, D. Zhao, Y. Gu, S. Memon, Z. Ren, B. Liu, X. Zhang, F. Xing, D. Li, Three-dimensional characterization of steel corrosion embedded in cement paste, Constr. Build. Mater. 143 (2017) 24–32.
[23] M. Stefanoni, U.M. Angst, B. Elsener, Kinetics of electrochemical dissolution of metals in porous media, Nature Mater. 1 (2019).
[24] B. Dong, G. Fang, Y. Liu, P. Dong, J. Zhang, F. Xing, S. Hong, Monitoring reinforcement corrosion and corrosion-induced cracking by X-ray microcomputed tomography method, Cem. Concr. Res. 100 (2017) 311–321.
[25] R. Zhang, A. Castel, R. François, The corrosion pattern of reinforcement and its influence on serviceability of reinforced concrete members in chloride environment, Cem. Concr. Res. 39 (2009) 1077–1086.
[26] T.A. Soylev, R. Francois, Quality of steel-concrete interface and corrosion of reinforcing steel, Cem. Concr. Res. 33 (2003) 1407–1415.
[27] C.L. Page, Initiation of chloride-induced corrosion of steel in concrete: role of the interfacial zone, Mater. Corros. 60 (2009) 586–592.
[28] A.T. Horne, I.G. Richardson, R.M.D. Brydson, Quantitative analysis of the microstructure of interfaces in steel reinforced concrete, Cem. Concr. Res. 37 (2007) 1613–1623.
[29] C.L. Page, Mechanism of corrosion protection in reinforced concrete marine structures, Nature, London 258 (11) (1975) 514–515.
[30] G. Glass, R. Yang, T. Dickhaus, N.R. Buenfeld, Backscattered electron imaging of the steel-concrete interface, Corros. Sci. 43 (2001) 605–610.
[31] G. Ebell, A. Burkert, J. Fischer, J. Lehmann, T. Müller, D. Meinel, O. Paetsch, Investigation of chloride-induced pitting corrosion of steel in concrete with innovative methods, Mater. Corrosion 67 (2016) 583–590.
[32] U. Angst, C.K. Larsen, Ø. Vennesland, B. Elsener, Influence of casting direction on chloride-induced rebar corrosion, in: P. Castro-Borges, E.I. Moreno, K. Sakai, O. Gjørv, N. Banthia (Eds.), CONSEC'10 6th Int. Conf. on Concrete under Severe Conditions, Environment and Loading, Taylor & Francis, London, 2010, pp. 359–366.